Journal of Molecular and Cellular Cardiology 157 (2021) 77–89

Contents lists available at ScienceDirect

Journal of Molecular and Cellular Cardiology

journal homepage: www.elsevier.com/locate/yjmcc

Translational investigation of electrophysiology in hypertrophic cardiomyopathy

Frederik Flenner [a,b], Christiane Jungen [b,c,d], Nadine Küpker [a], Antonia Ibel [a], Martin Kruse [e], Jussi T. Koivumäki [f], Anna Rinas [a], Antonia T.L. Zech [a,b], Alexandra Rhoden [a,b], Paul J. M. Wijnker [g], Marc D. Lemoine [b,c], Anna Steenpass [a], Evaldas Girdauskas [h], Thomas Eschenhagen [a,b], Christian Meyer [c,i,j], Jolanda van der Velden [g], Monica Patten-Hamel [k], Torsten Christ [a,b], Lucie Carrier [a,b,*]

[a] Institute of Experimental Pharmacology and Toxicology, Cardiovascular Research Center, University Medical Center Hamburg-Eppendorf, Hamburg, Germany
[b] DZHK (German Centre for Cardiovascular Research), partner site Hamburg/Kiel/Lübeck, Germany
[c] Department of Cardiology-Electrophysiology, cardiac Neuro- and Electrophysiology Research Group (cNEP), University Heart and Vascular Center, University Hospital Hamburg-Eppendorf, Hamburg, Germany
[d] Department of Cardiology, Willem Einthoven Center for Cardiac Arrhythmia Research and Management, Leiden University Medical Center, Leiden, the Netherlands
[e] Department of Biology and Program in Neuroscience, Bates College, Lewiston, ME, USA
[f] BioMediTech, Faculty of Medicine and Health Technology, Tampere University, Tampere, Finland
[g] Amsterdam UMC, Vrije Universiteit Amsterdam, Department of Physiology, Amsterdam Cardiovascular Sciences, Amsterdam, the Netherlands
[h] Department of Cardiovascular Surgery, University Heart and Vascular Center, University Hospital Hamburg-Eppendorf, Hamburg, Germany
[i] Division of Cardiology/Angiology/Intensiv Care, cardiac Neuro- and Electrophysiology Research Consortium (cNEP), EVK Düsseldorf, Teaching Hospital University of Düsseldorf, Düsseldorf, Germany
[j] Institute of Neural and Sensory Physiology, cardiac Neuro- and Electrophysiology Research Consortium (cNEP), University of Düsseldorf, Düsseldorf, Germany
[k] Department of General and Interventional Cardiology, University Heart Center, University Hospital Hamburg-Eppendorf, Hamburg, Germany

ARTICLE INFO

Keywords:
Hypertrophic cardiomyopathy
Sudden cardiac death
Cardiac arrhythmia
Mouse model
Engineered heart tissue
Action potential
Human tissue

ABSTRACT

Hypertrophic cardiomyopathy (HCM) patients are at increased risk of ventricular arrhythmias and sudden cardiac death, which can occur even in the absence of structural changes of the heart. HCM mouse models suggest mutations in myofilament components to affect Ca^{2+} homeostasis and thereby favor arrhythmia development. Additionally, some of them show indications of pro-arrhythmic changes in cardiac electrophysiology. In this study, we explored arrhythmia mechanisms in mice carrying a HCM mutation in *Mybpc3* (*Mybpc3*-KI) and tested the translatability of our findings in human engineered heart tissues (EHTs) derived from CRISPR/Cas9-generated homozygous *MYBPC3* mutant (*MYBPC3*hom) in induced pluripotent stem cells (iPSC) and to left ventricular septum samples obtained from HCM patients.

We observed higher arrhythmia susceptibility in contractility measurements of field-stimulated intact cardiomyocytes and ventricular muscle strips as well as in electromyogram recordings of Langendorff-perfused hearts from adult *Mybpc3*-KI mice than in wild-type (WT) controls. The latter only occurred in homozygous (Hom-KI) but not in heterozygous (Het-KI) mouse hearts. Both Het- and Hom-KI are known to display pro-arrhythmic increased Ca^{2+} myofilament sensitivity as a direct consequence of the mutation. In the electrophysiological characterization of the model, we observed smaller repolarizing K^+ currents in single cell patch clamp, longer ventricular action potentials in sharp microelectrode recordings and longer ventricular refractory periods in Langendorff-perfused hearts in Hom-KI, but not Het-KI. Interestingly, reduced K^+ channel subunit transcript levels and prolonged action potentials were already detectable in newborn, pre-hypertrophic Hom-KI mice. Human iPSC-derived *MYBPC3*hom EHTs, which genetically mimicked the Hom-KI mice, did exhibit lower mutant mRNA and protein levels, lower force, beating frequency and relaxation time, but no significant

Abbreviations: HCM, Hypertrophic cardiomyopathy; *Mybpc3*-KI (Het/Hom), *Mybpc3*-targeted knock-in mice (heterozygous / homozygous); iPSC, induced pluripotent stem cell; EHT, engineered heart tissue; SCD, sudden cardiac death; AP(D), action potential (duration).

* Corresponding author at: Institute of Experimental Pharmacology and Toxicology, University Medical Center Hamburg-Eppendorf, Martinistraße 52, 20246 Hamburg, Germany.
E-mail address: l.carrier@uke.de (L. Carrier).

https://doi.org/10.1016/j.yjmcc.2021.04.009
Received 10 March 2021; Received in revised form 14 April 2021; Accepted 29 April 2021
Available online 3 May 2021

alteration of the force-Ca^{2+} relation in skinned EHTs. Furthermore, *MYBPC3*hom EHTs did show higher spontaneous arrhythmic behavior, whereas action potentials measured by sharp microelectrode did not differ to isogenic controls. Action potentials measured in septal myectomy samples did not differ between patients with HCM and patients with aortic stenosis, except for the only sample with a *MYBPC3* mutation.

The data demonstrate that increased myofilament Ca^{2+} sensitivity is not sufficient to induce arrhythmias in the *Mybpc3*-KI mouse model and suggest that reduced K^+ currents can be a pro-arrhythmic trigger in Hom-KI mice, probably already in early disease stages. However, neither data from EHTs nor from left ventricular samples indicate relevant reduction of K^+ currents in human HCM. Therefore, our study highlights the species difference between mouse and human and emphasizes the importance of research in human samples and human-like models.

1. Introduction

Hypertrophic cardiomyopathy (HCM) is an inheritable disease which is passed on in an autosomal dominant way and has an estimated prevalence of 0.2% [1]. Most of the HCM cases are caused by mutations in genes encoding sarcomeric proteins [2], with the vast majority of mutations occurring in *MYBPC3* [3,4]. HCM is defined by left ventricular hypertrophy in the absence of obvious pathological reasons like hypertension or aortic stenosis. Hypertrophy in HCM is in general accompanied by myocardial disarray and fibrosis. HCM patients may suffer from syncope, general fatigue and dyspnea under exercise conditions and, if the disease progresses, heart failure. Another major complication associated with HCM are ventricular arrhythmias, which occurred in a non-sustained form in 20–30% of patients during Holter-monitoring [5,6]. These ventricular arrhythmias can cause sudden cardiac death (SCD) and may occur in young, previously undiagnosed and asymptomatic persons [7]. In line with this, HCM is seen as the major cause of SCD cases in young athletes [8]. While the annual rate of SCD in HCM patients has been estimated to be below 1% [9,10] and progress has been made to identify persons at SCD risk [7], SCD can occur in persons with hearts lacking hypertrophy or fibrosis, which can be a substrate for ventricular reentry circuits. This highlights the lack of knowledge about ventricular arrhythmia mechanisms in HCM and in general. One potential trigger for ventricular arrhythmias might be altered myofilament function [11], which is directly caused by HCM mutations. In addition, dysfunctions of cardiac ion channels, which might occur as a secondary effect of HCM, could cause fatal ventricular arrhythmias. Such channelopathies are in general seen as another major cause of SCD [12–15] and appear in ion channels which underlie the cardiac action potential (AP) or are important for the propagation of the excitatory signal in the heart [12,16]. Investigations in HCM mouse models, including models based on mutations in *MYBPC3*, found reduced expression of genes encoding K^+channel subunits [17,18]. Consequently, ventricular APs and QT intervals of these mice were prolonged. Prolonged APs related to decreased repolarizing K^+ currents and increased in both late Na^+ and Ca^{2+} currents have also been observed in HCM patient samples [19,20], and prolonged corrected QT (QT_c) intervals have predicted adequate ICD shocks in patients with established HCM [21]. Similarly, prolonged APs were related to increased Ca^{2+} currents in human induced pluripotent stem cell (iPSC)-derived engineered heart tissues (EHTs) from a HCM patient [22]. Prolonged APs were sensitive to diltiazem, which also normalized the prolonged QT_c interval of the index patient.

In this study, we evaluated if and how HCM-causing *MYBPC3* mutations translate into pro-arrhythmic changes of cardiac electrophysiology. Therefore, we investigated the electrophysiological properties of an HCM mouse model (*Mybpc3*-targeted knock-in [23]) with focus on occurrence of ventricular arrhythmias, AP repolarization and K^+ currents. We then tested the transferability of our findings to humans in both EHTs derived from human CRISPR/Cas9-generated homozygous *MYBPC3*-mutated iPSCs (*MYBPC3*hom) differentiated to cardiomyocytes, and in septal myectomy samples from HCM patients.

2. Methods

2.1. Animals

All experimental procedures were in accordance with the German Law for the Protection of Animals and with the guidelines of the European Union. Sacrifice of animals and harvesting of organs for experiments were performed following approved protocols accepted by the Ministry of Science and Public Health of the City State of Hamburg, Hamburg, Germany (organ extraction permit No. 653). The investigation conformed to the guide for the care and use of laboratory animals published by the National Institutes of Health (Bethesda, Maryland; Publication No. 85–23, revised 2011, published by National Research Council, Washington, D.C.).

The HCM model mice used in this study carries a G>A transition in the last nucleotide in exon 6 of *Mybpc3* at the heterozygous (Het-KI) or homozygous state (Hom-KI) [23]. This mutation is a HCM founder mutation (c.772G>A) in Tuscany, Italy, but is also detected in patients in other parts of the world and is associated with ICD implantation of SCD [24]. In mice, it causes an HCM-like phenotype whose degree depends on the zygosity. The mutation results in 3 different mutant mRNAs, one missense, one nonsense due to the skipping of exon 6 and one full-length as a result of the skipping of exon 6 plus the partial retention of intron 8 [23]. Het-KI and Hom-KI mice exhibited about 80% and 10% of the level of cMyBP-C in the WT heart, respectively [23]. Wild-type (WT) mice without the G>A transition from the same black-swiss strain were used as controls.

2.2. Human ventricular samples

All material was taken with informed consent of the patients and all procedures were in accordance with the Code of Ethics of the World Medical Association (Declaration of Helsinki). We received specimens of left ventricular septum myectomies of HCM patients in a completely anonymized way. These patients underwent surgery because of outflow tract obstruction of the left ventricle. As controls, we received small pieces from the same septum area which were removed during valve replacement operations in patients with aortic stenosis, which was approved by the local ethics committee in February 2017 (Nr. PV3759). All patients gave their informed consent for the usage of the tissue before the operation. One septal myectomy was derived from an HCM patient, carrying two genetic variants, one pathogenic mutation in *MYBPC3* (c.2234A>G; p.Asp745Gly) and one variant of unknown significance in *FLNC*, encoding filamin C (c.3004C>T; p.Arg1002Trp), also found in 3 controls in gnomAD database. This sample was therefore referred as *MYBPC3* sample. Muscle pieces were directly stored in ice-cold cardioplegic solution (mM: KCl 10; NaCl 100; KH_2PO_4 1.2; $MgSO_4$ 5; taurine 50; MOPS 5; glucose 20; 2,3-butanedione monoxime 30; pH 7.0) and transferred to the laboratory instantly where they were dissected into pieces for AP recordings and molecular biology analysis, the latter being snap-frozen in liquid nitrogen and stored at −80 °C.

2.3. Human iPSC-derived HCM cardiomyocytes and engineered heart tissues

Dermal fibroblasts were obtained from a control individual (ERC018). Reprogramming to iPSC was performed using CytoTune-iPS Sendai Reprogramming Kit 1.0 (Life Technologies) as previously described [22]. The human iPSCs were mutated in *MYBPC3* with Cas9 and sgRNA directed against exon 6 using CRISPR/Cas9 technology (Addgene PX458). Double strand breaks were induced at the desired locus using Cas9 nuclease guided by single guide (sg) RNAs without addition of a repair template. Mutated clones were screened for changes in the DNA sequence, which induce premature termination codons (PTC). One clone (*MYBPC3*hom) carried a homozygous T-insertion in exon 6 (c.768insT), which was expected to result in a frameshift and a PTC in exon 9. Correct modification of targeted sequences and absence of off-target changes were confirmed by sequencing, and correct karyotype was validated by G-banding and nanostring karyotype panel (data not shown).

Cardiomyocyte differentiation was performed according to previously published protocols [22,25,26]. After successful differentiation (coherent spontaneous beating in 2D culture and fraction of cardiac troponin T (cTnT)-positive cells above 60%), cells were either frozen or directly cast into EHT format as described previously [25,27]. EHTs were cultured for up to 62 days and monitored for contractility as described [25,27]. Whole EHTs were taken for AP measurements or snap-frozen in liquid nitrogen for RNA and protein quantification. Similar to the Hom-KI mice, the homozygous c.768insT gave rise to 2 mutant mRNAs in *MYBPC3*hom EHTs (supplemental Fig. 1A): 1) Mutant-1 mRNA is a nonsense mRNA containing the c.768insT, which induced a frameshift with 28 new amino acids and a PTC in exon 9 (p.Val256fsX28). Truncated 34 kDa protein was not detected by Western blot (data not shown); 2) Mutant 2 mRNA contains the T-insertion in exon 6 plus a retention of 38 nucleotides at the end of intron 8 (c.768insT/c.852-1insTCCCTCACTGCAGCCTCACTGGGGGTCCCTCTC-CATAG); this induced a 27-amino acid deletion and a 40-amino acid insertion with a reframing of the protein (p.Val256–27 amino acids +40 new amino acids in the M-motif, 1286 amino acids, 156 kDa mutant-2 protein, detected by Western blot). Therefore, *MYBPC3*hom EHTs mimicked the genetic situation of Hom-KI mice and exhibited markedly lower levels of both *MYBPC3* mRNA (supplemental Fig. 1B) and mutant-2 cMyBP-C (supplemental Fig. 1C) than isogenic control EHTs.

Force was measured of skinned EHTs as described before [28,29]. Shortly, EHTs were washed in cold PBS and removed from the silicone posts. Tissues were stored at −20 °C in a mixture of 50% glycerol and 50% relaxing solution (in mM: Na_2ATP 5.89, CrP 14.5, $MgCl_2$ 6.48, potassium propionate 40.76, BES 100, and EGTA 6.97, pH 7.1). Before force was measured, EHTs were incubated in relaxing solution containing 1% Triton X-100 for 18 h at 4 °C to permeabilize the membrane and EHT was cut into two strips (approximate 3.5 mm length, 0.45 mm width, $n = 5$ or 6 /group). The Ca^{2+} sensitivity of skinned EHT strips was measured using a permeabilized fiber test system (1400 A; Aurora Scientific). Strips were mounted between two T-clips and attached to a force transducer and a length controller. The strips were carefully stretched above slack length until they started to develop force when activated in pCa 4.5 solution (in mM: Na2ATP 5.97, CrP 14.5, MgCl2 6.28, potassium propionate 40.64, BES 100, and CaEGTA 7, pH 7.1) as described before [28,30]. After the initial activation step, strips were relaxed in pCa 9 buffer and exposed to solutions of increasing Ca^{2+} concentrations from pCa 9 to pCa 4.5. Force was measured in each pCa solution. Data were analyzed using the Hill equation, with pCa_{50} as the free Ca^{2+} concentration which yields 50% of the maximal force. The pCa_{50} represents the measure of myofilament Ca^{2+} sensitivity.

2.4. Mouse ventricular muscle strip force measurements

Freshly excised mouse hearts were submerged in cardioplegic solution (see 2.2). Atria were removed, the right ventricle was separated from the left ventricle and the left ventricle was separated into septum and free wall. The ventricular parts were then partitioned into two longitudinal (base to apex) strips each. They were then mounted between a steady clip and a force transducer in a temperature-controlled organ bath filled with modified oxygenated Tyrode's solution (mM: NaCl 126.7; KCl 5.4; $CaCl_2$ 1.8; $MgCl_2$ 1.05; $NaHCO_3$ 22; $NaHPO_4$ 0.42; glucose 5) warmed to 37 °C. Muscle strips were stimulated at 2 Hz 50% above stimulation threshold. Isoprenaline concentration-response curves were performed with cumulatively increasing concentrations ranging from 0.1 nM to 10 μM. Any additional contraction besides the 2-Hz rhythm was considered as arrhythmic.

2.5. Mouse ventricular cardiomyocyte preparation

Ventricular cardiomyocytes were isolated from adult mouse hearts as described previously [30,31]. In brief, freshly excised hearts were cannulated via the aorta and mounted on a temperature-controlled (37 °C) perfusion system. After retrograde perfusion with Ca^{2+}-free buffer solution (mM: NaCl 113; KCl 4.7; KH_2PO_4 0.6; Na_2HPO_4 0.6; MgSO4 1.2; $NaHCO_3$ 12; $KHCO_3$ 10; taurine 30; glucose 5.55; 2,3-butanedione monoxime 10; HEPES 10; pH 7.46) for 6.5 min, hearts were digested with 0.075 mg/mL Liberase TM (Roche Diagnostics, Mannheim, Germany) dissolved in buffer solution containing 12.5 μM $CaCl_2$ for 6–7 min. Ventricles were separated from the atria and carefully minced with forceps to dissociate single cardiomyocytes. Ca^{2+} was re-introduced stepwise to 1 mM. Isolated myocytes were then subsequently used for contractility analysis or patch clamp recordings.

2.6. Cell shortening analysis of mouse ventricular cardiomyocytes

Cells were perfused (rate 1 ml/min in a 400 μl chamber) with modified Tyrode's solution (mM: NaCl 135; KCl 4.7; KH_2PO_4 0.6; Na_2HPO_4 0.6; MgSO4 1.2; $CaCl_2$ 1.5; glucose 20; HEPES 10, pH 7.46) warmed to 37 °C. Cells were field-stimulated with 4 ms long 10 V pulses at 1 or 5 Hz pacing frequency. Before switching from 1 to 5 Hz, cells were superfused with 30 nM isoprenaline for 2–3 min until a new contractile steady-state was reached. Sarcomere shortening was assessed using a video-based sarcomere detection system and analyzed with the appendant software (IonWizard; IonOptix; Milton, MA, USA).

2.7. Langendorff-perfused mouse hearts

Whole heart electrophysiological parameters and arrhythmia susceptibility were tested ex vivo in Langendorff-perfused hearts as described previously [32]. In brief, freshly excised intact hearts were submerged in ice-cold Krebs-Henseleit solution (mM: NaCl 119, $NaHCO_3$ 25, KCl 4.6, KH_2PO_4 1.2, $MgSO_4$ 1.1, $CaCl_2$ 2.5, glucose 8.3 and Na-pyruvate 2; pH 7.4, 95% O_2/5% CO_2) and cannulated via the aorta. They were quickly attached to a temperature-controlled perfusion system and retrogradely perfused with a constant pressure of 80 mmHg. The right atrium was incised to allow insertion of an octapolar electrophysiology catheter (2F, CIB'ER Mouse, NuMed Inc., Hopkinton, NY, USA) into the right atrium and ventricle. Programmed stimulation was applied via the distal or proximal electrodes of the catheter using a designated digital stimulus generator (STG4002, Multi Channel Systems, Reutlingen, Germany) at twice the atrial or ventricular pacing threshold to determine standard electrophysiological parameters (atrial, ventricular and atrioventricular node refractory period, Wenckebach periodicity). A burst stimulation protocol (5 s of stimulation bursts with 50, 40, 30, 20 or 10 ms pacing cycle length with a 5 s pause in between) was applied to test susceptibility to ventricular arrhythmogenesis in hearts beating in their own sinus rhythm. The Langendorff-perfused mouse experiments were performed at 37 °C, and the baseline heart rate had to be above 350 bpm, otherwise the heart was not used in line with previously published protocol [33].

2.8. Action potential recordings in tissue (mouse and human heart, EHTs)

Freshly excised mouse hearts were submerged in cardioplegic solution (mM: KCl 10; NaCl 100; KH_2PO_4 1.2; $MgSO_4$ 5; taurine 50; MOPS 5; glucose 20; 2,3-butanedione monoxime 30; pH 7.0) and atria and right ventricle were removed. The left ventricle was partitioned in a septal and a free wall part. They were then fixated with the endocardial side upwards in an organ bath chamber which was perfused with oxygenated Tyrode's solution warmed to 37 °C. Human septal specimen were saved in cardioplegic solution directly after excision and quickly transferred to the lab. If big enough, some parts of the obtained specimen were separated and saved for molecular analysis. The rest was trimmed for the AP measurements and fixated in a Tyrode's solution-perfused organ bath. Human EHTs were directly transferred from cell culture to the organ bath and fixed there. The preparations were field stimulated (baseline frequencies: mouse: 5 Hz, human septum: 1 Hz, EHTs: 2 Hz) 50% above stimulation threshold. Action potentials were recorded as previously described [34,35] with sharp microelectrodes (tip resistance of 20–40 MΩ).

2.9. K^+ and Ca^{2+} current recordings

Isolated adult ventricular mouse cardiomyocytes were used for whole-cell K^+ current recordings following the previously published protocol [18]. The cells were kept in bath solution (mM: NaCl 136; KCl 4; $MgCl_2$ 2; $CaCl_2$ 1; $CoCl_2$ 5; tetrodotoxin (TTX) 0.02; Hepes 10; glucose 10; pH 7.4; 300 mosmol l^{-1}) at 37 °C. Pipettes had tip resistances of 2–5 MΩ and contained in mM: KCl 135; EGTA 10; Hepes 10; K_2ATP 5; glucose 5; pH 7.2; 310 mosmol l^{-1}. Voltage-activated outward K^+ currents were evoked by a 4.5 s long depolarizing voltage step to +40 mV from a holding potential of −70 mV. Inwardly directed K^+ currents were evoked by a subsequent 4.5 s long voltage step to −120 mV. To dissect amplitudes of the individual K^+ current components $I_{to,f}$, $I_{to,s}$, $I_{K,slow}$ and I_{ss}, three exponential functions were fitted to outward current traces with the ANA-3 software (MFK, Niedernhausen, Germany): $A \times e^{\frac{-x}{\tau 1}} + B \times e^{\frac{-x}{\tau 2}} + C \times e^{\frac{-x}{\tau 3}} + D$.The amplitudes (A: $I_{to,f}$, B: $I_{to,s}$, C: $I_{K,slow}$, D: I_{ss}) of the K^+ current components were calculated with the help of to their individual inactivation time constants (tau values; τ1: $I_{to,f}$, τ2: $I_{to,s}$, τ3: $I_{K,slow}$) [36].-

For Ca^{2+} current measurements, cells were kept in bath solution (mM: tetraethyl ammonium chloride 140; glucose 10; 4-aminopyridine 3; $CaCl_2$ 1.8, $MgCl_2$ 1; HEPES 10; pH 7.4) at 21–23 °C. The pipette solution contained in mM: $CsCl_2$ 120, $MgCl_2$ 1, EGTA 10, MgATP 4, HEPES 5 at a pH of 7.2. Whole-cell L-type Ca^{2+} currents were evoked by depolarizing voltage steps from a holding potential of −80 mV to −50 to +70 mV. At the end of the measurement, 1 μM nifedipine was applied to validate specificity of L-type Ca^{2+} current measurements.

2.10. Action potential simulations

Simulations were run with an established in silico model of a mouse ventricular myocyte [37]. For the WT, the normal cell model variant was employed, using a standard current stimulus pacing protocol. To recapitulate the electrophysiological HCM phenotype, the digital cell was reparameterized by the following fold changes in ion current conductances: $I_{Na} = 1.07$, $I_{to,f} = 0.40$, $I_{Kur1} = 0.57$, $I_{Kur} = 0.60$, $I_{Kss} = 0.69$; $I_{Ca,L} = 1.17$. In all simulations, the digital cell was paced for 5 min at the set BCL to reach a quasi-steady state before storage of the data from a single action potential for analysis. Simulations were run with the commercial MATLAB software (release 2017b), using the built-in function (ode15s) to solve the differential equations.

2.11. mRNA level quantification

Adult and neonatal mouse hearts, human septum and EHT samples were snap-frozen in liquid nitrogen after excision and either stored at −80 °C or directly homogenized and RNA was extracted using the SV total RNA isolation system (Promega, Z3105) or TriZol (ambion, 15,596,018). Quantification of mRNA levels was performed with customized nanoString Gene Expression CodeSets as described previously [38,39].

2.12. Protein quantification

Proteins from mouse hearts, human septum and EHTs were extracted by homogenizing the tissue in self-made (30 mM Tris-(hydroxymethyl)-aminoethane, 5 mM ethylene diamine tetraacetic acid, 30 mM NaF, 3% sodium dodecyl sulfate, 10% glycerin) or commercial protein extraction buffer (M-PER, Thermo scientific, 8503). The debris was spun down and the supernatant used as whole protein extract. Proteins were mixed with Laemmli buffer (30 mM Tris-HCl pH 6.8, 300 mM dithiothreitol, 6% sodium dodecyl sulfate, 0.03% bromophenol blue, 30% gycerol) and heated for 5–10 min at 95 °C for denaturation, then separated on SDS poly-acrylamide gels (10%) and blotted onto nitrocellulose membranes with wet Western Blot technique at 300 mA for 90 min. Total proteins were visualized with Ponceau staining, target proteins were stained with primary antibodies (anti cMyBP-C, dilution 1:1000, Santa Cruz sc-137,181; anti cardiac troponin T (cTnT), dilution 1:6000, Abcam ab10218) overnight after blocking unspecific binding sites with 5% milk powder in TBS-Tween for 1 h. The following day, respective horse radish peroxidase-conjugated secondary antibodies (anti mouse HRP, dilution 1:10000, Dianova 515–035-003) were applied for 1 h and signals were detected using chemiluminescent substrates (SuperSignal®, Thermo Scientific, 34,076 or Clarity™, BIO-RAD, 170–5061) in a ChemiDoc™ Touch System (BIO-RAD). Quantification of the signals was done using the respective software.

2.13. Statistical analysis

All data are expressed as mean ± SEM. Curve fitting and statistical analysis were performed using the GraphPad Prism 8 software (GraphPad Software, USA). Where possible, data sets were tested for normality and lognormality and the appropriate statistical test was chosen accordingly [40]. For Fig. 4, we did perform a nested 1-way ANOVA, which considered both the number of animals and the number of cardiomyocytes per animal as previously described [41,42]. Used statistical tests are indicated in the respective graphs.

3. Results

3.1. Increased arrhythmia susceptibility in Mybpc3-KI mouse hearts, ventricular muscle strips and cardiomyocytes

During force measurements in isolated ventricular mouse cardiomyocytes and muscle strip preparations, we noticed a tendency towards more arrhythmic (e.g. additional or lacking) contractions in Het-KI and Hom-KI preparations than in their WT counterparts, especially when challenged with β-adrenergic stimulation and/or high pacing frequencies (supplemental Fig. 2A, B). Notably, the Ca^{2+} sensitizer EMD57033, which increases myofilament Ca^{2+} sensitivity, a hallmark of the mutations in Het-KI and Hom-KI cardiomyocytes [43], increased the percentage of arrhythmic events in WT cardiomyocytes. Similar to EMD57033, the voltage-gated K^+ channel inhibitor 4-aminopyridine (4-AP) increased the susceptibility to arrhythmias when challenged with isoprenaline in WT muscles strips, albeit the EC_{50} for isoprenaline was significantly higher than in Hom-KI ($P = 0.0044$; supplemental Fig. 2B). This suggests that increased myofilament Ca^{2+} sensitivity and/or alteration of K^+ channel currents contribute to arrhythmias in mouse cardiomyocytes.

To test if increased arrhythmia susceptibility also occurs in whole hearts from *Mybpc3*-KI mice, we challenged them with a burst pacing

protocol (Fig. 1A). In Hom-KI hearts, stimulation bursts frequently triggered ventricular tachycardia events (VT; ≥ extra beats after burst; Fig. 1B, C). These events often transformed into long-lasting (>1 min) monomorphic tachycardias, which were not self-terminating, but had to be interrupted by overdrive pacing. In contrast, in WT and Het-KI hearts, the stimulation bursts rarely triggered VTs. Programmed stimulation revealed significantly longer ventricular refractory periods in Hom-KI (31.2 ± 2.3 ms in Hom-KI vs 26.3 ± 3.5 ms in WT and 23.6 ± 2.2 ms in Het-KI, Fig. 1D). Atrial refractory periods were shorter in Het-KI and to a lesser extent in Hom-KI (27.2 ± 1.8 ms in WT, 24.8 ± 1.8 ms in Hom-KI and 24 ± 1.4 ms in Het-KI, supplemental Fig. 2C) than in WT. Other electrophysiological parameters (e.g. Wenckebach Point, supplemental Fig. 2D) did not differ between the genotypes.

3.2. Prolonged action potentials in Hom-KI left ventricle

To evaluate whether prolonged refractoriness in HCM mouse heart is caused by differences in repolarization, we performed AP measurements with sharp microelectrodes in left ventricular (LV) preparations of WT, Het-KI and Hom-KI mice. APs measured in the LV endocardium were significantly longer in hearts from 30-week-old Hom-KI mice than from from Het-KI and WT mice (Fig. 2A–C). Slowing of repolarization was already visible in early phases of the AP and persisted until late phases (APD_{20}: 7.5 ± 3.5 ms in Hom-KI vs. 4.8 ± 1.8 ms in WT and 3.5 ± 1.1 ms in Het-KI, APD_{70}: 29.2 ± 8.5 ms in Hom-KI vs. 20.9 ± 8.7 ms in WT and 22.1 ± 5.5 ms in Het-KI). To test if repolarization is affected before the development of cardiac hypertrophy and dysfunction [44–46], we repeated the measurements in hearts from postnatal day 1 (P1) Hom-KI mice. Again, AP duration (APD) was longer in Hom-KI LV endocardium throughout the whole repolarization phase (APD_{20}: 11.9 ± 5.6 ms in KI vs. 7.6 ± 3.2 ms in WT, APD_{70}: 28.9 ± 9.3 ms in Hom-KI vs. 22.8 ± 8 ms in WT, Fig. 2D–F).

3.3. Reduced mRNA levels of K^+ channel subunits in Hom-KI mouse hearts

In order to test if abnormalities of repolarization in Hom-KI mice are caused by altered gene expression of ion channels, we developed a panel of specific Nanostring nCounter probes for known ion channel-related gene products. Especially gene expression of several K^+ channel subunits was aberrant in Hom-KI, with the I_{to} component coding genes *Kcnd2* and *Kcnd3* being lower, whereas the mRNA level of *Kcna5* encoding I_{KUR} was higher in adult Hom-KI than in WT (Fig. 3A). In neonatal P1 mice, both *Kcnd2* and *Kcnd3* RNA counts were lower in Hom-KI than WT (Fig. 3B). In contrast to adult mice, *Kcnj11* and *Kcnj12* mRNA levels were lower in Hom-KI than WT P1 mice (Fig. 3B).

3.4. Reduced K^+ currents in Hom-KI mouse ventricular myocytes

To test if the reduced expression of genes encoding K^+ channels results in a decline in K^+ currents, which could explain prolongation of the AP, we measured K^+ currents in whole-cell patch-clamped adult ventricular mouse cardiomyocytes. The peak component of the outward current was lower in Hom-KI than in WT and Het-KI (Peak: Hom-KI 43.9 ± 5.8 pA/pF vs. WT 73.8 ± 11.9 pA/pF and Het-KI 75.7 ± 6.7 pA/pF; Fig. 4B, D). The late component, measured at the end of the test pulse did not differ between the groups: Hom-KI 10.5 ± 1.9 pA/pF vs. WT 16.4 ± 3.6 pA/pF and Het-KI 21.3 ± 2.5 pA/pF (Fig. 4B, E). Fitting of three exponential functions to outward current traces revealed that all outward current components were smaller in Hom-KI than WT, with $I_{to,f}$ and $I_{K,slow}$ being significantly smaller ($P < 0.05$, Kruskal-Wallis test followed by Dunn's multiple comparison test, Fig. 4F). The inwardly rectifying current I_{K1} tended to be lower in Hom-KI than in WT cardiomyocytes as well, but this was not statistically significant (Fig. 4C).

In further electrophysiological analysis of the model, we saw that maximum upstroke velocity of APs, which started on average from similar resting membrane potentials (supplemental Fig. 3C, D), did not differ between the groups (supplemental Fig. 3A, B). From this we

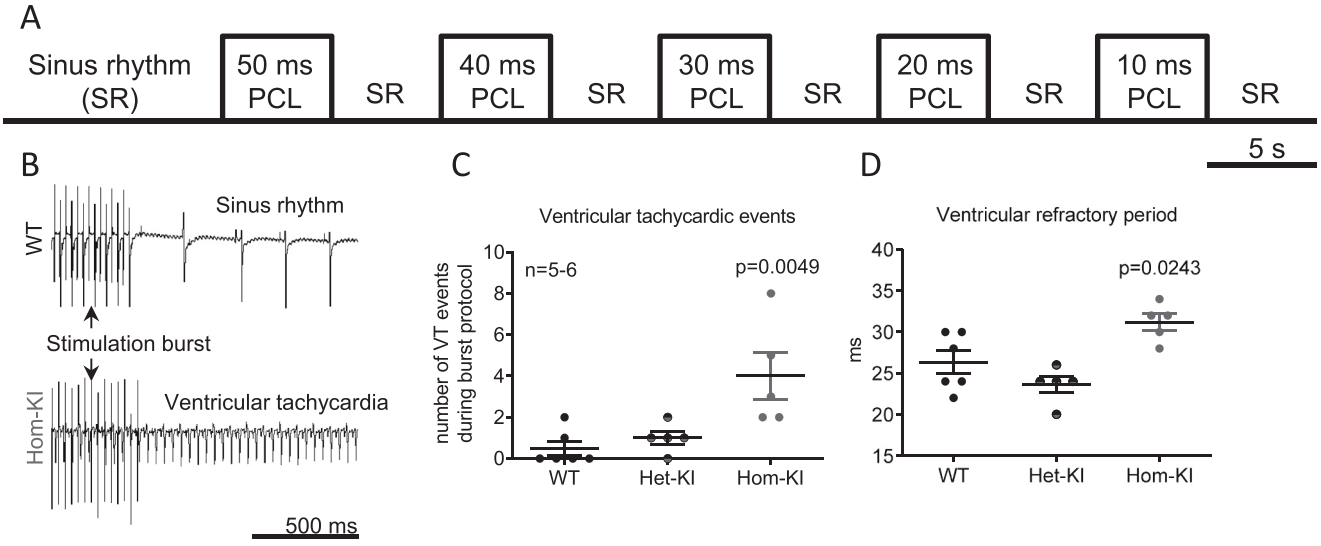

Fig. 1. Ventricular tachycardias in Langendorff-perfused mouse hearts.
A: Burst pacing protocol for Langendorff-perfused hearts with decreasing burst pacing cycle lengths.
B: Representative traces of electromyograms recorded in a WT heart (top) which went back to sinus rhythm after an episode of burst pacing and in a Hom-KI heart (bottom) which had an episode of sustained ventricular tachycardia after a stimulation burst.
C: Number of tachycardic events in hearts of different genotypes, which were challenged to the complete burst stimulation protocol.
D: Ventricular refractory period times in hearts of different genotypes. Stimulation protocol: S1: 12 × 100 ms, S2.
Data are expressed as mean ± SEM. *P* values vs. WT were obtained with 1-way ANOVA, followed by Dunnett's multiple comparison test.
Abbreviations: Het-KI, heterozygous *Mybpc3*-targeted knock-in; Hom-KI, homozygous *Mybpc3*-targeted knock-in; PCL, pacing cycle length; VT, ventricular tachycardia; WT, wild-type.

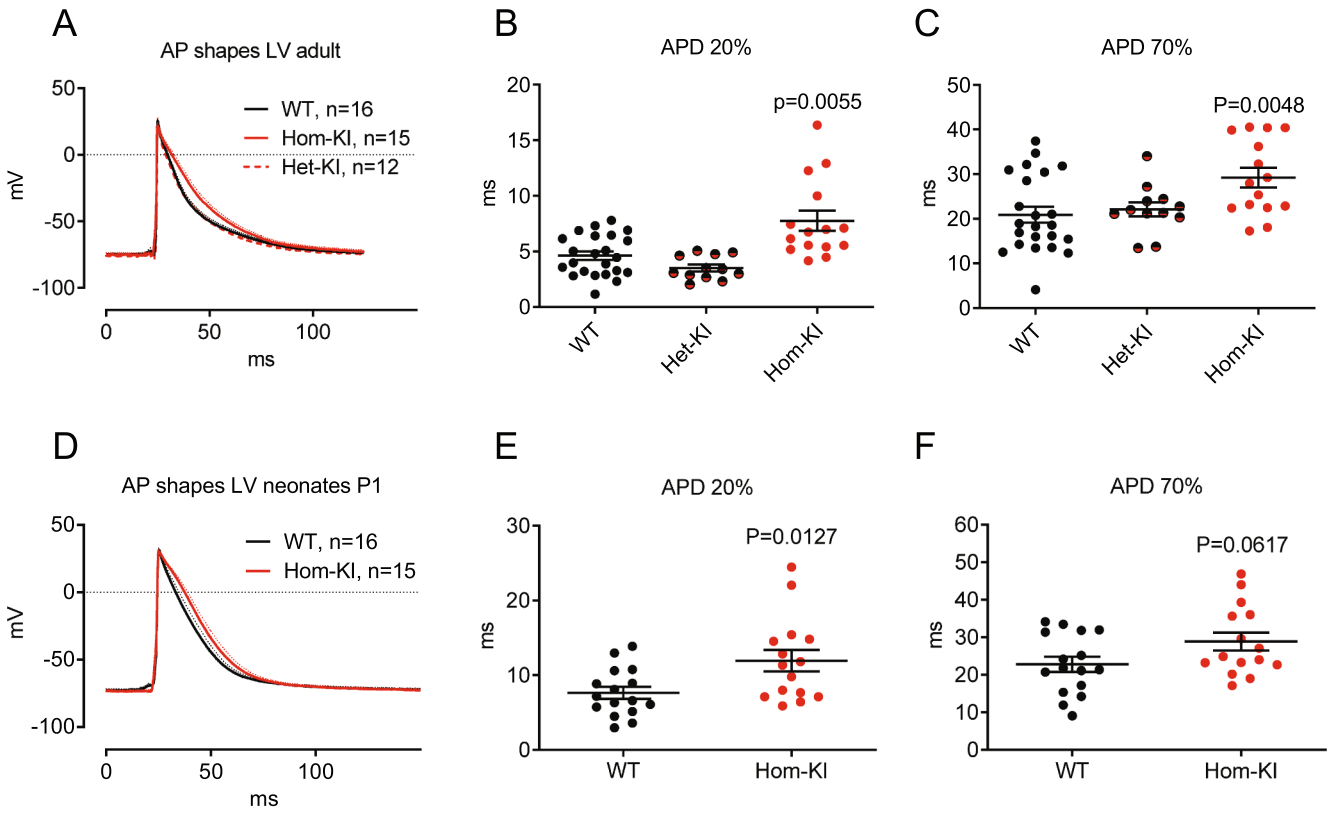

Fig. 2. Action potentials measured in subendocardial layers of the left ventricle of mouse hearts.
A: Action potentials measured in LV of adult mouse hearts (averaged traces from different animals, dotted lines indicate SEM).
B: Quantification of action potential duration at 20% of repolarization measured in adult mouse hearts of different genotypes.
C: Quantification of action potential duration at 70% of repolarization measured in adult mouse hearts of different genotypes.
D: Action potentials measured in LV of neonatal mouse hearts (averaged traces from different animals, dotted lines indicate SEM).
E: Quantification of action potential duration at 20% of repolarization measured in neonatal mouse hearts of different genotypes.
F: Quantification of action potential duration at 70% of repolarization measured in neonatal mouse hearts of different genotypes.
Date are expressed as mean ± SEM, *P* values vs. WT were obtained with the Kruskal-Wallis test, followed by Dunn's multiple comparison test (panels B and C) or with the unpaired Student's *t*-test (panels E and F).
Abbreviations: AP, action potential; APD, action potential duration; Het-KI, heterozygous *Mybpc3*-targeted knock-in; Hom-KI, homozygous *Mybpc3*-targeted knock-in; LV, left ventricle; n, number of mice; WT, wild type.

concluded that the Na^+ currents did not differ between the genotypes. We additionally evaluated the Ca^{2+} current density and their current-voltage relationships in the absence and presence of isoprenaline (1 μM) in adult ventricular cardiomyocytes, but did not see significant differences between WT and Hom-KI (supplemental Fig. 3E, F). We included all obtained electrophysiological data for Na^+, K^+ and Ca^{2+} currents in an in silico simulation of a mouse ventricular AP and obtained a similar prolongation in Hom-KI compared to WT like in the sharp microelectrode recordings (supplemental Fig. 3G).

Taken together, the data indicated a loss of repolarizing K^+ currents in Hom-KI that leads to prolonged APs and a prolonged refractory period. This change constitutes an arrhythmogenic substrate and appears to occur prior to the development of cardiac hypertrophy in this model.

3.5. Functional measurements in intact and skinned human engineered heart tissues

Given the known differences in cardiac electrophysiology between mice and men, we tested the translatability of our findings in human iPSC-derived EHTs carrying a homozygous T insertion in exon 6 (c.768insT, *MYBPC3*hom) and compared them to the isogenic control cell line from which they were generated with CRISPR/Cas9. The *MYBPC3*hom EHTs therefore mimicked the genetic situation of the Hom-KI mice, and, such as the Hom-KI mice [23], showed a markedly lower levels of mutant *MYBPC3* mRNAs and cMyBP-C protein (supplemental Fig. 1). We evaluated the force amplitude and kinetics of *MYBPC3*hom and control EHTs over time. Force amplitude was higher (Fig. 5A) and relaxation time at 80% of relaxation ($RT_{80\%}$) was often lower (Fig. 5B) in *MYBPC3*hom than in isogenic control EHTs. Higher force development was associated with lower beating frequency of *MYBPC3*hom than control EHTs (Fig. 5C). These contractile abnormalities are in agreement with previous findings obtained in EHTs derived from Hom-KI neonatal mice [28].

We also evaluated the RR-scatter, which represents the interdecile range of mean beat-to-beat distance in unpaced EHTs (Fig. 5D). An increase in RR-scatter reflects arrhythmic behavior in EHTs. *MYBPC3*hom EHTs exhibited a higher RR-scatter than control EHTs over time (significant at days 13 and 20). On the other hand, *MYBPC3*hom EHTs did not exhibit difference to isogenic controls in arrhythmic events when challenged with 100 nM isoprenaline (data not shown).

To evaluate whether the *MYBPC3*hom EHTs developed higher myofilament Ca^{2+} sensitivity, we evaluated the force-pCa relation in skinned EHTs. *MYBPC3*hom EHTs showed a slight left-shift of the force-pCa relation (Fig. 5E), higher F_{max} (Fig. 5F), a non-significantly higher myofilament Ca^{2+} sensitivity (=higher pCa_{50}; Fig. 5G), and a slightly lower (non-significant) nHill coefficient (Fig. 5H). Taken together, force development was higher in both intact and skinned *MYBPC3*hom than

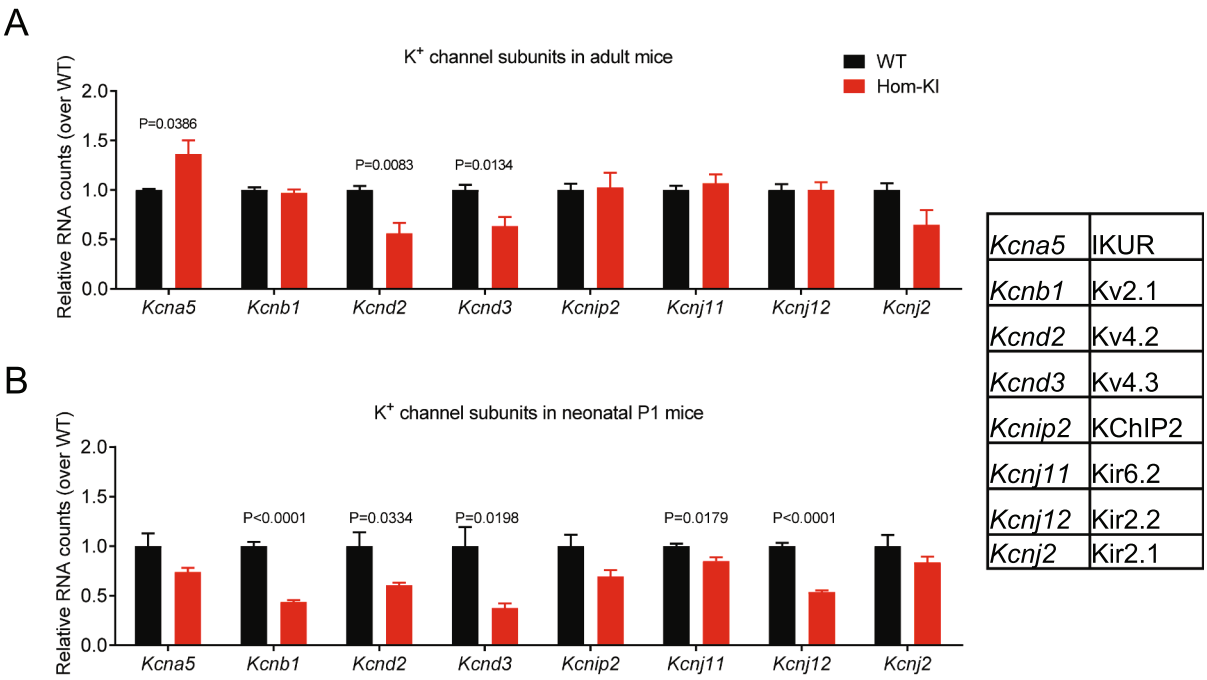

Fig. 3. Quantification of mRNA levels of potassium channel subunits in murine ventricular samples.
A: mRNA levels of K^+ channel subunits in left ventricular samples from adult Hom-KI and WT mouse hearts.
B: mRNA levels of K^+ channel subunits in ventricular samples from neonatal Hom-KI and WT mouse hearts.
Data are expressed as mean ± SEM. *P* values vs. WT were obtained with the unpaired Student's *t*-test ($n = 4$ samples per group).
Channels encoded by the respective genes are given as abbreviations in the inset table.
Abbreviations: Hom-KI, homozygous *Mybpc3*-targeted knock-in (red bars); P1, postnatal day 1; WT, wild-type (black bars)

isogenic EHTs. *MYBPC3*hom skinned EHTs did have a slightly higher myofilament Ca^{2+} sensitivity, but not statistically significant. This supports previous data obtained for other human HCM EHTs or septal myectomies [22,47]. Relaxation time was shorter in *MYBPC3*hom EHTs, exhibiting a low amount of cMyBP-C, which is in agreement with previous findings in EHTs derived from neonatal Hom-KI cardiac cells [28,48].

3.6. Action potential measurements in human EHTs and in LV samples of HCM and AoS samples

We recorded the APs, measured by sharp microelectrodes in human EHTs. APs did not differ in duration between *MYBPC3*hom and isogenic control EHTs (Fig. 6A–C). Noteworthy, maximum upstroke velocities were significantly lower and take-off potentials were slightly higher in *MYBPC3*hom than isogenic controls (supplemental Fig. 4). This suggests that electrophysiological characteristics of *MYBPC3*hom EHTs substantially differ from those of Hom-KI mice. Evaluation of the expression of K^+ channels with a customized NanoString human panel showed a markedly lower *KCNA4*, *KCNA5*, *KCNE1*, *KCNH2*, *KCNJ2* in *MYBPC3*hom than control EHTs, and, in addition, lower expression of *CACNA1C*, *CACNA1G* and SCN5A in *MYBPC3*hom than control EHTs (Supplemental Fig. 7).

We also performed sharp microelectrode AP recordings in fresh LV septal myectomy samples of HCM patients with outflow tract obstruction and used samples from patients undergoing surgical correction of aortic stenosis (AoS) as controls. Hypertrophy- and arrhythmia-related patient data as well as medication are indicated in supplemental Table 1. APs did not significantly differ between HCM and AoS samples (Fig. 6D–F). Interestingly, however, the AP of the only *MYBPC3* sample was markedly longer than all other HCM (not evaluated for gene defect) and AoS samples and was associated with a higher maximum upstroke velocity (Supplemental Fig. 4F), suggesting that this *MYBPC3* mutation may prolong APD and therefore contribute to arrhythmias in the HCM patient. Notably, ex vivo APD_{90} measured in myectomy samples from patients with HCM did not correlate with septum thickness measured by echocardiography (supplemental Fig. 5).

4. Discussion

In this study, we investigated the relationship between HCM-causing mutations and their impact on cardiac electrophysiology and the development of arrhythmias in three different models. In the homozygous, but not in heterozygous *Mybpc3*-KI mouse model, we found reduced K^+ conductivity, prolongation of ventricular APs and refractory periods and increased arrhythmia susceptibility. As these prolonged APs and reduced K^+ channel transcript levels also occurred in pre-hypertrophic mice, our findings suggest reduced K^+ currents as one of the arrhythmia mechanisms in HCM, which occurs independent from hypertrophy. On the other hand, we did not find prolonged APs in human iPSC-derived EHTs bearing a homozygous *MYBPC3* mutation and in septal myectomy samples taken from HCM patients, except for one sample carrying a pathogenic *MYBPC3* mutation.

In Hom-KI mice, we found higher susceptibility to arrhythmias in the whole heart and muscle strips and a clear trend towards more arrhythmia in single cardiomyocytes. In contrast, Het-KI showed no arrhythmias in Langendorff-perfused hearts. Apparently, the previously reported elevated myofilament Ca^{2+} sensitivity, which occurs in both Hom-KI and Het-KI mice [43] and is considered to be pro-arrhythmic (reviewed in [11,49]), was not sufficient to induce arrhythmias in burst-paced whole Het-KI hearts. Obviously, reduced K^+ currents in Hom-KI hearts were needed to evoke arrhythmias in burst-paced intact hearts. However, as we did not include β-adrenergic stimulation in the Langendorff-perfused hearts, we cannot exclude that Het-KI hearts also have increased arrhythmia susceptibility under isoprenaline. Likewise, we cannot conclude if increased myofilament Ca^{2+} sensitivity is a

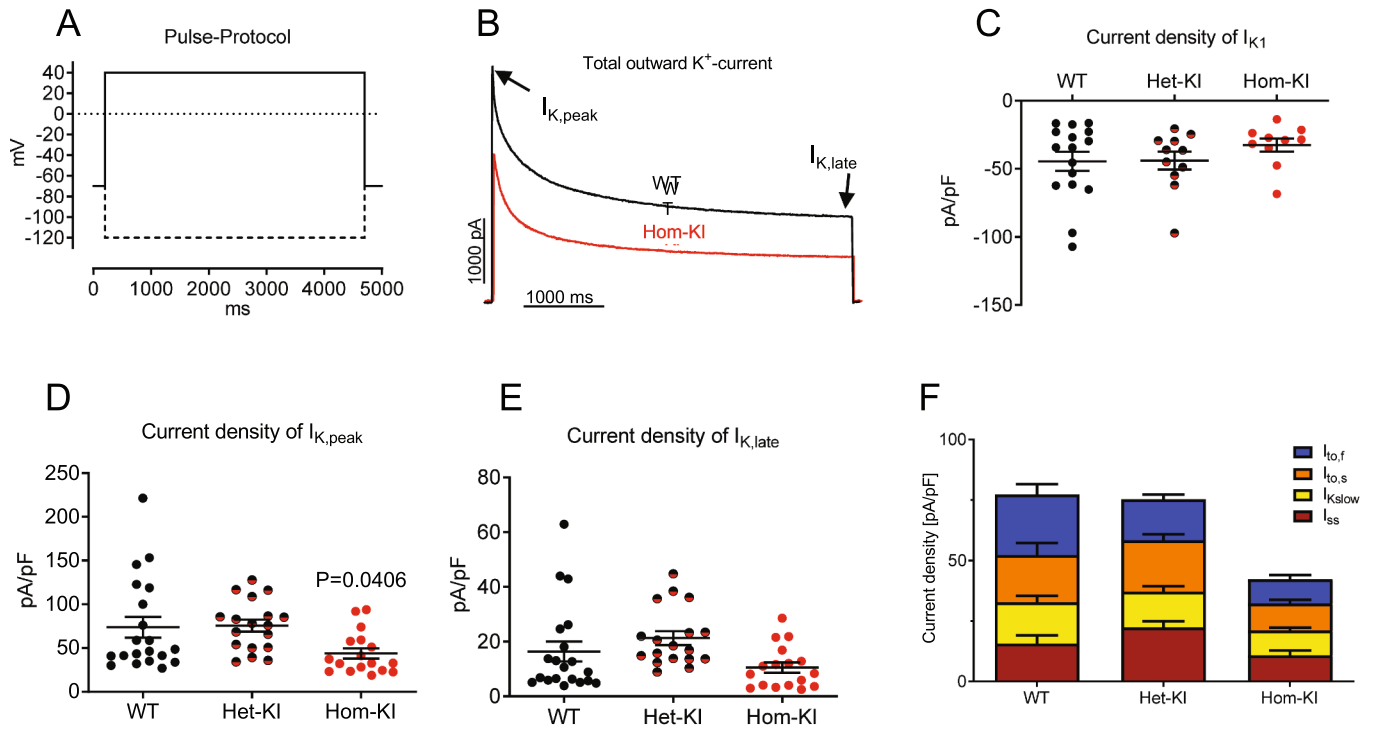

Fig. 4. Potassium currents in isolated adult ventricular mouse cardiomyocytes.
A: Recording protocol. Outward currents were recorded first, inward currents were recorded at the end of the protocol by hyperpolarizing the cell (dashed line).
B: Representative traces of recordings of outward currents from a WT (black) and a Hom-KI (red) cardiomyocyte.
C: Current densities of I_{K1} in ventricular adult cardiomyocytes of different genotypes (WT: N/*n* = 9/16, Het-KI: N/*n* = 5/10, Hom-KI: N/*n* = 5/11).
D: Current densities of $I_{K,peak}$ in ventricular adult cardiomyocytes of different genotypes (WT: N/*n* = 10/20, Het-KI: N/*n* = 5/18, Hom-KI: N/*n* = 7/17).
E: Current densities of $I_{K,late}$ in ventricular adult cardiomyocytes of different genotypes (WT: *n* = 10/20, Het-KI: *n* = 5/18, Hom-KI: *n* = 7/17).
F: Different components of outward K^+ currents calculated by three-exponential curve fit (WT: *n* = 10/20, Het-KI: *n* = 5/18, Hom-KI: *n* = 7/17).
Data are expressed as mean ± SEM, with *P* values vs. WT were obtained with the nested 1-way ANOVA, followed by Dunnett's multiple comparison test.
Abbreviations: Het-KI, heterozygous *Mybpc3*-targeted knock-in; Hom-KI, homozygous *Mybpc3*-targeted knock-in; N/*n*, number of mice/cardiomyocytes; WT, wild type.

prerequisite for K^+ current decline-associated arrhythmias in Hom-KI. Here, it has to be considered that many HCM-causing mutations lead to a problematically increased energy demand [50,51], which can be induced by elevated myofilament Ca^{2+} sensitivity and aggravate under β-adrenergic stimulation. This has been shown to result in induction of arrhythmias [52]. However, the observation that reduced K^+ conductivity can be a pro-arrhythmic trigger in HCM mouse models has been made before [17,18]. In silico modelling of ventricular mouse APs, which includes all electrophysiological data obtained in this study, demonstrates that the observed aberrancies in K^+ currents are sufficient to explain the longer APD in Hom-KI mice (supplemental Fig. 3G), and therefore most likely the prolonged ventricular refractory period as well. We additionally observed that these aberrancies already exist directly after birth in a pre-hypertrophic stage, with the constraint that we did not perform single cardiomyocyte electrophysiology from neonatal mice because of technical difficulties. As pro-arrhythmic alterations in ion channel expression has already been observed in neonatal *Mybpc3* null mice [53], our findings led to the hypothesis that arrhythmic events in pre-hypertrophic HCM patients might actually be caused by a reduced K^+ channel expression and function. Unfortunately, the rapid disease progression in the Hom-KI mice [44,45] (and the very mild phenotype in Het-KI mice) make it very difficult to retrace the process by which a mutation in *Mybpc3* leads to electrophysiological changes in K^+ currents.

We therefore tried to shed further light on the relationship between HCM mutations and K^+ channel function by investigating human iPSC-derived EHTs carrying a homozygous *MYBPC3* mutation (*MYBPC3*hom), reproducing the gene defect and related molecular consequences of Hom-KI mice (much lower levels of mutant mRNA and protein). While there is ongoing concern whether human iPSC-derived cardiomyocytes are limited as a model because of their low maturity, this can be improved, especially concerning left ventricular-like electrophysiology, when cultured in 3-dimensional EHTs [54,55]. Accordingly, our recordings show high similarity between AP shapes from EHTs and septal human heart probes (Fig. 6 and supplemental Fig. 6). However, in contrast to the mouse model and to a recent HCM study by our group based on a missense mutation in *ACTN2* [22], we did not see difference in APD between *MYBPC3*hom and isogenic control EHTs. Quantification of ion channel mRNAs revealed lower transcript levels for *KCNA4*, *KCNA5* (carrying Kv1.4 and Kv1.5, which constitute I_{to} currents) and *KCNJ2* (Kir2.1, carrying I_{K1}) in *MYBPBC3*hom than in isogenic control EHTs (supplemental Fig. 7). As especially I_{to} is far less important in human than in rodent ventricle, a potential reduction of this current might have much smaller impact on AP shape. In line with this assumption, we recently demonstrated that contribution of transient potassium outward currents like I_{Kur} and I_{to} to repolarization is rather small in EHTs [56]. However, *MYBPBC3*hom EHTs had lower amount of *SCN5A* and *CACNA1C* transcripts, as well as slower upstroke velocities, combined with a slightly more positive take-off potential of the AP than isogenic controls. This suggests that the potential reduction in transient K^+ currents might not have an impact on AP in *MYBPBC3*hom EHTs because it could be counterbalanced by lower depolarizing Na^+ and Ca^{2+} currents. On the other hand, human *MYBPC3*hom EHTs exhibited lower beating frequency and higher RR-scatter that reflects arrhythmic behaviors, which are in agreement with previous findings in mouse Hom-KI EHTs [28], suggesting that a low level of mutant cMyBP-C

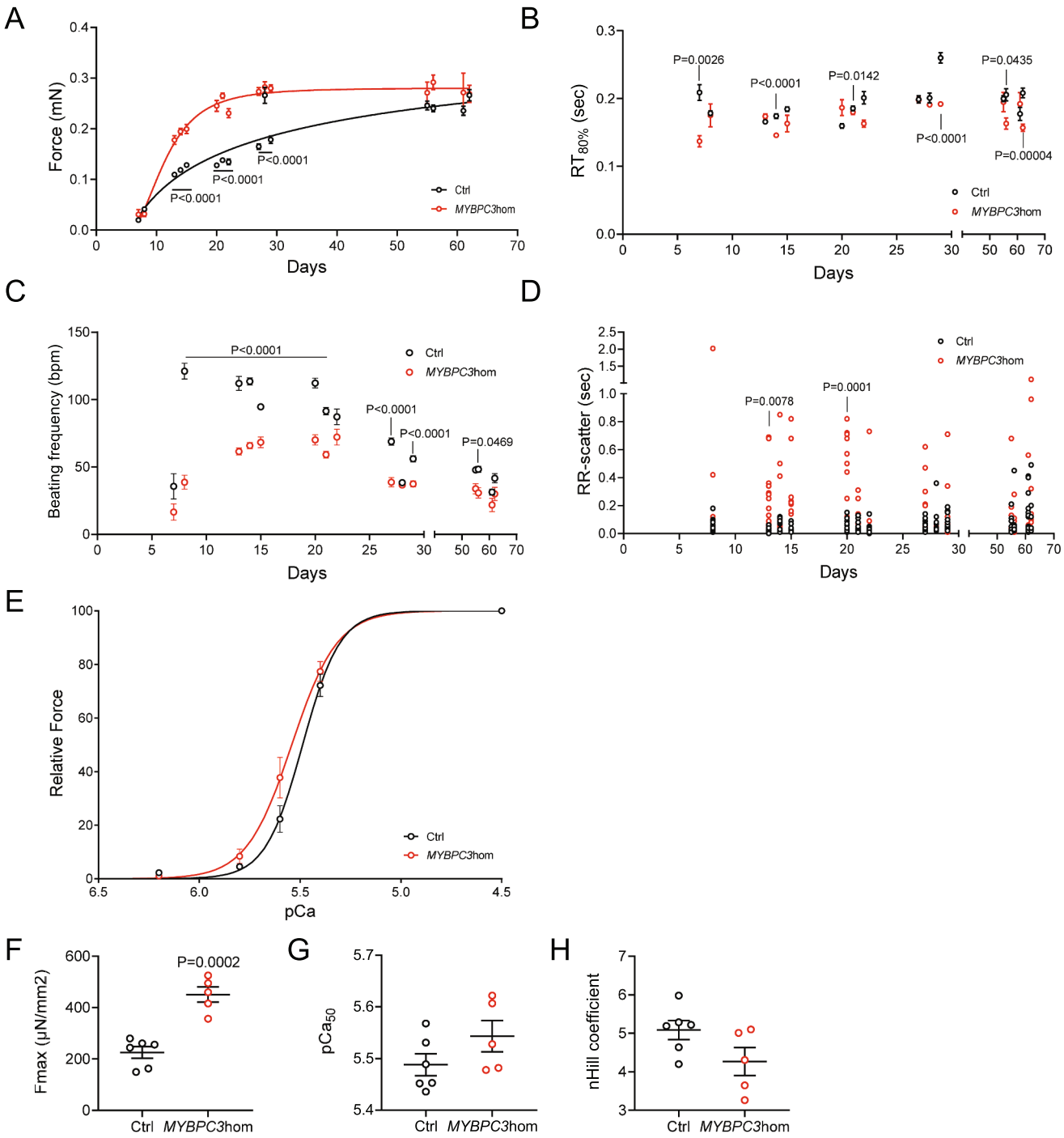

Fig. 5. Contractility measurements overtime in human engineered heart tissues (EHTs).
Measurements were performed overtime in *MYBPC3*hom (red) and isogenic control (Ctrl, black) EHTs.
A: Force development in human EHTs.
B. Relaxation time at 80% of relaxation in human EHTs.
C. Spontaneous beating frequency in human EHTs.
D. Arrhythmic behavior (determined by the RR-scatter) in human EHTs.
E. Force-pCa relation in human skinned EHTs.
F. Maximal Force obtained in skinned human EHTs.
G. pCa_{50} in skinned human EHTs.
H. nHill coefficient in skinned human EHTs.
Data are expressed as mean ± SEM, with *P* values vs. Ctrl obtained with a 2-way ANOVA, followed by Sidak's multiple comparison test (Panels A-D) or unpaired Student's *t*-test (Panels F—H). In Panels A-D, $n = 24$ Ctrl and n = 21 *MYBPC3*hom until day 22, $n = 15$ Ctrl and n = 14 *MYBPC3*hom until day 29, and $n = 11$ Ctrl and n = 7 *MYBPC3*hom until day 62), in panels F—H, $n = 6$ Ctrl and n = 5 *MYBPC3*hom).

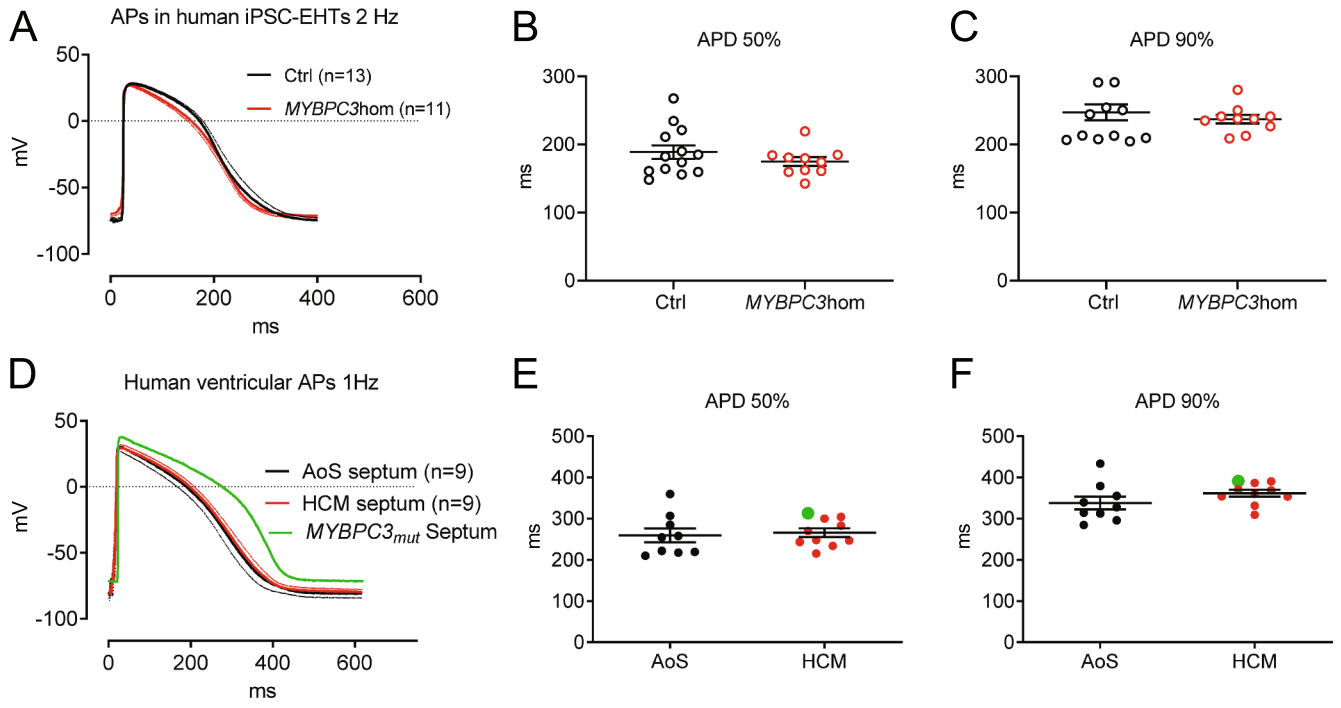

Fig. 6. Action potentials measured in human engineered heart tissue and ventricular septum specimen.
A: Action potentials measured in human isogenic control (black) and *MYBPC3*hom (red) EHTs (averaged traces ±SEM).
B: Quantification of action potential duration at 50% repolarization measured in EHTs of different genotypes.
C: Quantification of action potential duration at 90% repolarization measured in EHTs of different genotypes.
D: Action potentials measured in LV septum samples of HCM and aortic stenosis patients (averaged traces ±SEM). Parts of this data set have been published previously [44].
E: Quantification of action potential duration at 50% repolarization measured in patient samples.
F: Quantification of action potential duration at 90% repolarization measured in patient samples.
In Panels B, C, E, F, data are expressed as mean ± SEM.
Curve and dots in green in panels D—F correspond to the data obtained in a patient sample carrying a *MYBPC3* mutation.
Abbreviations: AoS, aortic stenosis; APD, action potential duration; ctrl, isogenic control; EHTs, engineered heart tissues; *MYBPC3*hom, homozygous *MYBPC3* T-insertion

protein as found in both homozygous human and mouse models is associated with this phenotype [28]. Similarly, intact or skinned *MYBPC3*hom EHTs developed higher maximal force and faster relaxation time, in agreement with previous findings obtained in EHTs derived from neonatal Hom-KI or Hom-knock-out (KO) cardiac cells [28,29,48]. The shorter relaxation time in all these models with a low amount of cMyBP-C is consistent with the shortening of the ejection phase of systole in Hom-KO mice [57] and supports the role of cMyBP-C in sustaining the dynamic range of myosin-actin interaction during contraction twitch [31,57–59].

The results from the AP recordings in EHTs are in line with the results obtained in human septal myectomy samples, except for the only *MYBPC3*-mutated sample that showed a markedly longer AP than all other HCM and AoS samples (Fig. 6D). This suggests that this *MYBPC3* mutation may prolong APD and therefore contribute to arrhythmias in the HCM patient, which could be related to the previously measured higher myofilament Ca^{2+} sensitivity [47]. For the other HCM samples, however, the APD did not significantly differ to samples from patients with aortic stenosis. This contradicts previous findings of profoundly longer APD in single cells isolated from HCM myectomy samples [19,20]. However, the authors did not specify in their legend which gene defects were associated with the prolonged APDs. These previous studies used control cohorts of patients with variable indications (aortic stenosis, regurgitation, mitral valve steno-insufficiency, aortic valve stenosis or insufficiency) and without clear septal hypertrophy (< 14 mm septal thickness). Our control consists of patients with aortic stenosis with an averaged interventricular septal thickness of 13.4 mm (range: 10–18 mm; HCM: average 22.3 mm, range 16–29 mm). However, the main difference between our and the former studies occurs in the HCM groups, in which we obtained APD values similar to those in the respective control groups of all studies. A second major difference is technical: while the former studies measured APs in patch-clamped cardiomyocytes enzymatically dissociated from septal specimen and paced at 0.2–1 Hz, we measured APs in intact muscle under physiological conditions at pacing frequencies at ≥1 Hz. We believe that the latter approach is less artefact-prone and better reflects intact physiology. Nevertheless, we cannot judge in how far measurements of APs in a very unique piece of septum allow inferences to APs in other parts of the left ventricle. However, it is noteworthy that like in the *Mybpc3*-KI mice, the degree of hypertrophy did not correlate with APD - while in non-hypertrophied neonatal mouse hearts APs were prolonged, they were not prolonged in hypertrophied human HCM septum.

5. Limitations of the study and conclusion

While the mouse model is based on a founder mutation in HCM patients and reproduces many aspects of HCM, the disease progression (very mild, non-progressing phenotype in heterozygous animals vs. almost immediate onset after birth in homozygous animals) makes it difficult to differentiate between early and late disease stages. Some severe electrophysiological changes in the homozygous animals have potentially already happened in embryonic development [60,61], which

seems unlikely in human adult heterozygous patients. On the other hand, although we have substantial evidence for pro-arrhythmic changes directly after birth, we cannot exclude that development of hypertrophy is needed as an additional trigger for arrhythmia occurrence on whole heart level. Indeed, there are many other potential mechanisms such as Ca^{2+} leak, alternans, alterations in connexin expression, increased reactive oxygen species that may contribute to the arrhythmogenic phenotype [62]. Additionally, it is noteworthy that we generated a homozygous *MYBPC3*-mutant iPSC line to mimic the consequence of the mutation in the Hom-KI mice, while adult patients carry heterozygous mutations. Here, we have to search for relevant methods, triggers and readouts to enhance the usefulness of this model in HCM and arrhythmia research. The majority of the study is based on mutations in *Mybpc3/MYBPC3*, and we only had the genetic data for one HCM individual carrying a *MYBPC3* mutation. In addition, we cannot exclude that the control group consisting of aortic stenosis patients have altered cardiac electrophysiology as well. As the control samples were very small, they had to be used completely for AP recordings, after which they could not be used for reliable molecular biological analysis anymore. Therefore, we cannot provide mRNA quantification data for the septum specimen.

In summary, we did not find substantial evidence that a reduction of repolarizing K^+ currents, which occurred in our and other HCM mouse models, is a general pro-arrhythmic mechanism in human HCM. While transcript levels provided evidence of reduced K^+ ion channel subunits in the *MYBPC3*hom EHTs, this did not translate into visible abnormalities in the AP. Besides the aforementioned other potential abnormalities in Na^+ and Ca^{2+} channels in the *MYBPC3*hom EHTs, the reason for the absence of AP irregularities in the human EHT models and human specimens might be the low impact of early repolarization in native human ventricular and engineered ventricular-like tissue. Cardiac electrophysiology differs particularly in this regard between mice and humans (for review, see [63]), therefore a reduction in currents like $I_{to,f}$, which apparently had a big impact in the mouse model, simply does not affect the human ventricular AP significantly. This is supported by the notion that the typical notch in the AP, which is caused by early repolarizing currents, was almost absent in measured APs of both human EHTs and septum specimen. Whether a reduction of repolarizing currents may affect other parts of the ventricle, in which contribution of early repolarization is much larger, remains to be elucidated.

Funding

This work was supported by the German Research Foundation (Deutsche Forschungsgemeinschaft, DFG, project number 316865582 to FF), the DZHK (German Centre for Cardiovascular Research to LC), the German Ministry of Research Education (BMBF to LC), the European Research Council Advanced Grant (IndivuHeart, 340248, to T.E.), the German Foundation for Heart Research (project F/51/17 to A.T.L.Z.), the Academy of Finland Centre of Excellence in Body-on-Chip Research, the Finnish Foundation for Cardiovascular Research, the Paavo Nurmi Foundation and the Pirkanmaa Regional Fund of the Finnish Cultural Foundation (all to J.K.).

Declaration of competing interest

None.

Acknowledgements

We would like to thank Dr. Giulia Mearini and Elisabeth Kraemer (Hamburg) for karyotyping of the hiPSC clones. We thank vecteezy.com for vector graphics of mouse and humans used in the graphical abstract. We thank Michiel van Wijhe, Stefan Conijn, and Zubayda Sultan (AMC Amsterdam) for the help in the preparation of samples and for measurements of force-Ca^{2+} relation in human skinned EHTs.

Appendix A. Supplementary data

Supplementary data to this article can be found online at https://doi.org/10.1016/j.yjmcc.2021.04.009.

References

[1] C. Semsarian, J. Ingles, M.S. Maron, B.J. Maron, Reply: what is the true prevalence of hypertrophic cardiomyopathy? J. Am. Coll. Cardiol. 66 (2015) 1846–1847.
[2] M. Akhtar, P. Elliott, The genetics of hypertrophic cardiomyopathy, Glob. Cardiol. Sci. Pract. 2018 (2018) 36.
[3] L. Carrier, Targeting the population for gene therapy with MYBPC3, J. Mol. Cell. Cardiol. 150 (2020) 101–108.
[4] P.M. Elliott, A. Anastasakis, M.A. Borger, M. Borggrefe, F. Cecchi, P. Charron, A. A. Hagege, A. Lafont, G. Limongelli, H. Mahrholdt, W.J. McKenna, J. Mogensen, P. Nihoyannopoulos, S. Nistri, P.G. Pieper, B. Pieske, C. Rapezzi, F.H. Rutten, C. Tillmanns, H. Watkins, 2014 ESC Guidelines on diagnosis and management of hypertrophic cardiomyopathy: the Task Force for the Diagnosis and Management of Hypertrophic Cardiomyopathy of the European Society of Cardiology (ESC), Eur. Heart J. 35 (2014) 2733–2779.
[5] L. Monserrat, P.M. Elliott, J.R. Gimeno, S. Sharma, M. Penas-Lado, W.J. McKenna, Non-sustained ventricular tachycardia in hypertrophic cardiomyopathy: an independent marker of sudden death risk in young patients, J. Am. Coll. Cardiol. 42 (2003) 873–879.
[6] A.S. Adabag, S.A. Casey, M.A. Kuskowski, A.G. Zenovich, B.J. Maron, Spectrum and prognostic significance of arrhythmias on ambulatory Holter electrocardiogram in hypertrophic cardiomyopathy, J. Am. Coll. Cardiol. 45 (2005) 697–704.
[7] P. Jorda, A. Garcia-Alvarez, Hypertrophic cardiomyopathy: sudden cardiac death risk stratification in adults, Glob. Cardiol. Sci. Pract. 25 (2018).
[8] B.J. Maron, J.J. Doerer, T.S. Haas, D.M. Tierney, F.O. Mueller, Sudden deaths in young competitive athletes: analysis of 1866 deaths in the United States, 1980-2006, Circulation 119 (2009) 1085–1092.
[9] P.M. Elliott, J.R. Gimeno, R. Thaman, J. Shah, D. Ward, S. Dickie, M.T. Tome Esteban, W.J. McKenna, Historical trends in reported survival rates in patients with hypertrophic cardiomyopathy, Heart 92 (2006) 785–791.
[10] B.J. Maron, Contemporary insights and strategies for risk stratification and prevention of sudden death in hypertrophic cardiomyopathy, Circulation 121 (2010) 445–456.
[11] S. Huke, Linking myofilaments to sudden cardiac death: recent advances, J. Physiol. 595 (2017) 3939–3947.
[12] O. Campuzano, C. Allegue, S. Partemi, A. Iglesias, A. Oliva, R. Brugada, Negative autopsy and sudden cardiac death, Int. J. Legal Med. 128 (2014) 599–606.
[13] O. Campuzano, O. Sanchez-Molero, C. Allegue, M. Coll, I. Mademont-Soler, E. Selga, C. Ferrer-Costa, J. Mates, A. Iglesias, G. Sarquella-Brugada, S. Cesar, J. Brugada, J. Castella, J. Medallo, R. Brugada, Post-mortem genetic analysis in juvenile cases of sudden cardiac death, Forensic Sci. Int. 245 (2014) 30–37.
[14] C. Allegue, R. Gil, A. Blanco-Verea, M. Santori, M. Rodriguez-Calvo, L. Concheiro, A. Carracedo, M. Brion, Prevalence of HCM and long QT syndrome mutations in young sudden cardiac death-related cases, Int. J. Legal Med. 125 (2011) 565–572.
[15] M.J. Ackerman, S.G. Priori, S. Willems, C. Berul, R. Brugada, H. Calkins, A. J. Camm, P.T. Ellinor, M. Gollob, R. Hamilton, R.E. Hershberger, D.P. Judge, H. Le Marec, McKenna WJ, E. Schulze-Bahr, C. Semsarian, J.A. Towbin, H. Watkins, A. Wilde, C. Wolpert, D.P. Zipes, S. Heart Rhythm, A. European Heart Rhythm, HRS/EHRA expert consensus statement on the state of genetic testing for the channelopathies and cardiomyopathies: this document was developed as a partnership between the Heart Rhythm Society (HRS) and the European Heart Rhythm Association (EHRA), Europace 13 (2011) 1077–1109.
[16] A. Fernandez-Falgueras, G. Sarquella-Brugada, J. Brugada, R. Brugada, O. Campuzano, Cardiac channelopathies and sudden death: recent clinical and genetic advances, Biology (Basel) 6 (2017).
[17] A. Toib, C. Zhang, G. Borghetti, X. Zhang, M. Wallner, Y. Yang, C.D. Troupes, H. Kubo, T.E. Sharp, E. Feldsott, R.M. Berretta, N. Zalavadia, D.M. Trappanese, S. Harper, P. Gross, X. Chen, S. Mohsin, S.R. Houser, Remodeling of repolarization and arrhythmia susceptibility in a myosin-binding protein C knockout mouse model, Am. J. Physiol. Heart Circ. Physiol. 313 (2017) H620–H630.
[18] R. Hueneke, A. Adenwala, R.L. Mellor, J.G. Seidman, C.E. Seidman, J.M. Nerbonne, Early remodeling of repolarizing K(+) currents in the alphaMHC(403/+) mouse model of familial hypertrophic cardiomyopathy, J. Mol. Cell. Cardiol. 103 (2017) 93–101.
[19] R. Coppini, C. Ferrantini, L. Yao, P. Fan, M. Del Lungo, F. Stillitano, L. Sartiani, B. Tosi, S. Suffredini, C. Tesi, M. Yacoub, I. Olivotto, L. Belardinelli, C. Poggesi, E. Cerbai, A. Mugelli, Late sodium current inhibition reverses electromechanical dysfunction in human hypertrophic cardiomyopathy, Circulation 127 (2013) 575–584.
[20] C. Ferrantini, J.M. Pioner, L. Mazzoni, F. Gentile, B. Tosi, A. Rossi, L. Belardinelli, C. Tesi, C. Palandri, R. Matucci, E. Cerbai, I. Olivotto, C. Poggesi, A. Mugelli, R. Coppini, Late sodium current inhibitors to treat exercise-induced obstruction in hypertrophic cardiomyopathy: an in vitro study in human myocardium, Br. J. Pharmacol. 175 (2018) 2635–2652.
[21] B. Gray, J. Ingles, C. Medi, C. Semsarian, Prolongation of the QTc interval predicts appropriate implantable cardioverter-defibrillator therapies in hypertrophic cardiomyopathy, JACC Heart Fail 1 (2013) 149–155.

[22] M. Prondzynski, M.D. Lemoine, A.T. Zech, A. Horvath, V. Di Mauro, J. T. Koivumaki, N. Kresin, J. Busch, T. Krause, E. Kramer, S. Schlossarek, M. Spohn, F.W. Friedrich, J. Munch, S.D. Laufer, C. Redwood, A.E. Volk, A. Hansen, G. Mearini, D. Catalucci, C. Meyer, T. Christ, M. Patten, T. Eschenhagen, L. Carrier, Disease modeling of a mutation in alpha-actinin 2 guides clinical therapy in hypertrophic cardiomyopathy, EMBO Mol. Med. 11 (2019), e11115.
[23] N. Vignier, S. Schlossarek, B. Fraysse, G. Mearini, E. Kramer, H. Pointu, N. Mougenot, J. Guiard, R. Reimer, H. Hohenberg, K. Schwartz, M. Vernet, T. Eschenhagen, L. Carrier, Nonsense-mediated mRNA decay and ubiquitin-proteasome system regulate cardiac myosin-binding protein C mutant levels in cardiomyopathic mice, Circ. Res. 105 (2009) 239–248.
[24] E.S. Singer, J. Ingles, C. Semsarian, R.D. Bagnall, Key value of RNA analysis of MYBPC3 splice-site variants in hypertrophic cardiomyopathy, Circ. Genom. Precis Med. 12 (2019), e002368.
[25] K. Breckwoldt, D. Letuffe-Breniere, I. Mannhardt, T. Schulze, B. Ulmer, T. Werner, A. Benzin, B. Klampe, M.C. Reinsch, S. Laufer, A. Shibamiya, M. Prondzynski, G. Mearini, D. Schade, S. Fuchs, C. Neuber, E. Kramer, U. Saleem, M.L. Schulze, M. L. Rodriguez, T. Eschenhagen, A. Hansen, Differentiation of cardiomyocytes and generation of human engineered heart tissue, Nat. Protoc. 12 (2017) 1177–1197.
[26] D. Mosqueira, I. Mannhardt, J.R. Bhagwan, K. Lis-Slimak, P. Katili, E. Scott, M. Hassan, M. Prondzynski, S.C. Harmer, A. Tinker, J.G.W. Smith, L. Carrier, P. M. Williams, D. Gaffney, T. Eschenhagen, A. Hansen, C. Denning, CRISPR/Cas9 editing in human pluripotent stem cell-cardiomyocytes highlights arrhythmias, hypocontractility, and energy depletion as potential therapeutic targets for hypertrophic cardiomyopathy, Eur. Heart J. 39 (2018) 3879–3892.
[27] I. Mannhardt, K. Breckwoldt, D. Letuffe-Breniere, S. Schaaf, H. Schulz, C. Neuber, A. Benzin, T. Werner, A. Eder, T. Schulze, B. Klampe, T. Christ, M.N. Hirt, N. Huebner, A. Moretti, T. Eschenhagen, A. Hansen, Human engineered heart tissue: analysis of contractile force, Stem Cell Rep. 7 (2016) 29–42.
[28] A. Stohr, F.W. Friedrich, F. Flenner, B. Geertz, A. Eder, S. Schaaf, M.N. Hirt, J. Uebeler, S. Schlossarek, L. Carrier, A. Hansen, T. Eschenhagen, Contractile abnormalities and altered drug response in engineered heart tissue from Mybpc3-targeted knock-in mice, J. Mol. Cell. Cardiol. 63C (2013) 189–198.
[29] P.J. Wijnker, F.W. Friedrich, A. Dutsch, S. Reischmann, A. Eder, I. Mannhardt, G. Mearini, T. Eschenhagen, J. van der Velden, L. Carrier, Comparison of the effects of a truncating and a missense MYBPC3 mutation on contractile parameters of engineered heart tissue, J. Mol. Cell. Cardiol. 97 (2016) 82–92.
[30] F. Flenner, F.W. Friedrich, N. Ungeheuer, T. Christ, B. Geertz, S. Reischmann, S. Wagner, K. Stathopoulou, K.D. Sohren, F. Weinberger, E. Schwedhelm, F. Cuello, L.S. Maier, T. Eschenhagen, L. Carrier, Ranolazine antagonizes catecholamine-induced dysfunction in isolated cardiomyocytes, but lacks long-term therapeutic effects in vivo in a mouse model of hypertrophic cardiomyopathy, Cardiovasc. Res. 109 (2016) 90–102.
[31] L. Pohlmann, I. Kroger, N. Vignier, S. Schlossarek, E. Kramer, C. Coirault, K. R. Sultan, A. El-Armouche, S. Winegrad, T. Eschenhagen, L. Carrier, Cardiac myosin-binding protein C is required for complete relaxation in intact myocytes, Circ. Res. 101 (2007) 928–938.
[32] C. Jungen, K. Scherschel, C. Eickholt, P. Kuklik, N. Klatt, N. Bork, T. Salzbrunn, F. Alken, S. Angendohr, C. Klene, J. Mester, N. Klocker, M.W. Veldkamp, U. Schumacher, S. Willems, V.O. Nikolaev, C. Meyer, Disruption of cardiac cholinergic neurons enhances susceptibility to ventricular arrhythmias, Nat. Commun. 8 (2017) 14155.
[33] C. Jungen, K. Scherschel, N.I. Bork, P. Kuklik, C. Eickholt, H. Kniep, N. Klatt, S. Willems, V.O. Nikolaev, C. Meyer, Impact of intracardiac neurons on cardiac electrophysiology and arrhythmogenesis in an Ex Vivo langendorff system, J. Vis. Exp. 22 (135) (2018) 57617.
[34] E. Wettwer, O. Hala, T. Christ, J.F. Heubach, D. Dobrev, M. Knaut, A. Varro, U. Ravens, Role of IKur in controlling action potential shape and contractility in the human atrium: influence of chronic atrial fibrillation, Circulation 110 (2004) 2299–2306.
[35] M.D. Lemoine, T. Krause, J.T. Koivumaki, M. Prondzynski, M.L. Schulze, E. Girdauskas, S. Willems, A. Hansen, T. Eschenhagen, T. Christ, Human induced pluripotent stem cell-derived engineered heart tissue as a sensitive test system for QT prolongation and arrhythmic triggers, Circ. Arrhythm. Electrophysiol. 11 (2018), e006035.
[36] T. Christ, E. Wettwer, N. Voigt, O. Hala, S. Radicke, K. Matschke, A. Varro, D. Dobrev, U. Ravens, Pathology-specific effects of the IKur/Ito/IK,ACh blocker AVE0118 on ion channels in human chronic atrial fibrillation, Br. J. Pharmacol. 154 (2008) 1619–1630.
[37] S. Morotti, A.G. Edwards, A.D. McCulloch, D.M. Bers, E. Grandi, A novel computational model of mouse myocyte electrophysiology to assess the synergy between Na+ loading and CaMKII, J. Physiol. 592 (2014) 1181–1197.
[38] I. Mannhardt, A. Eder, B. Dumotier, M. Prondzynski, E. Kramer, M. Traebert, K. D. Sohren, F. Flenner, K. Stathopoulou, M.D. Lemoine, L. Carrier, T. Christ, T. Eschenhagen, A. Hansen, Blinded contractility analysis in hiPSC-cardiomyocytes in engineered heart tissue format: comparison with human atrial trabeculae, Toxicol. Sci. 158 (2017) 164–175.
[39] M. Prondzynski, E. Kramer, S.D. Laufer, A. Shibamiya, O. Pless, F. Flenner, O. J. Muller, J. Munch, C. Redwood, A. Hansen, M. Patten, T. Eschenhagen, G. Mearini, L. Carrier, Evaluation of MYBPC3 trans-splicing and gene replacement as therapeutic options in human iPSC-derived cardiomyocytes, Mol. Ther. Nucleic Acids 7 (2017) 475–486.
[40] D. Ismaili, B. Geelhoed, T. Christ, Ca(2+) currents in cardiomyocytes: how to improve interpretation of patch clamp data? Prog. Biophys. Mol. Biol. 157 (2020) 33–39.
[41] M.B. Sikkel, D.P. Francis, J. Howard, F. Gordon, C. Rowlands, N.S. Peters, A. R. Lyon, S.E. Harding, K.T. MacLeod, Hierarchical statistical techniques are necessary to draw reliable conclusions from analysis of isolated cardiomyocyte studies, Cardiovasc. Res. 113 (2017) 1743–1752.
[42] D.A. Eisner, Pseudoreplication in physiology: more means less, J. Gen. Physiol. 153 (2021).
[43] B. Fraysse, F. Weinberger, S.C. Bardswell, F. Cuello, N. Vignier, B. Geertz, J. Starbatty, E. Kramer, C. Coirault, T. Eschenhagen, J.C. Kentish, M. Avkiran, L. Carrier, Increased myofilament Ca(2+) sensitivity and diastolic dysfunction as early consequences of Mybpc3 mutation in heterozygous knock-in mice, J. Mol. Cell. Cardiol. 52 (2012) 1299–1307.
[44] C. Gedicke-Hornung, V. Behrens-Gawlik, S. Reischmann, B. Geertz, D. Stimpel, F. Weinberger, S. Schlossarek, G. Precigout, I. Braren, T. Eschenhagen, G. Mearini, S. Lorain, T. Voit, P.A. Dreyfus, L. Garcia, L. Carrier, Rescue of cardiomyopathy through U7snRNA-mediated exon skipping in Mybpc3-targeted knock-in mice, EMBO Mol. Med. 5 (2013) 1128–1145.
[45] G. Mearini, D. Stimpel, B. Geertz, F. Weinberger, E. Krämer, S. Schlossarek, J. Mourot-Filiatre, A. Stöhr, A. Dutshc, P.J.M. Wijnker, I. Braren, H.A. Katus, O. J. Müller, T. Voit, T. Eschenhagen, L. Carrier, *Mybpc3* gene therapy for neonatal cardiomyopathy enables longterm disease prevention in mice, Nat. Commun. 5 (2014) 5515.
[46] G. Mearini, D. Stimpel, E. Kramer, B. Geertz, I. Braren, C. Gedicke-Hornung, G. Precigout, O.J. Muller, H.A. Katus, T. Eschenhagen, T. Voit, L. Garcia, S. Lorain, L. Carrier, Repair of Mybpc3 mRNA by 5′-trans-splicing in a mouse model of hypertrophic cardiomyopathy, Mol. Ther. Nucleic Acids 2 (2013), e102.
[47] N. Kresin, S. Stucker, E. Kramer, F. Flenner, G. Mearini, J. Munch, M. Patten, C. Redwood, L. Carrier, F.W. Friedrich, Analysis of contractile function of permeabilized human hypertrophic cardiomyopathy multicellular heart tissue, Front. Physiol. 10 (2019) 239.
[48] A. Dutsch, P.J.M. Wijnker, S. Schlossarek, F.W. Friedrich, E. Kramer, I. Braren, M. N. Hirt, D. Breniere-Letuffe, A. Rhoden, I. Mannhardt, T. Eschenhagen, L. Carrier, G. Mearini, Phosphomimetic cardiac myosin-binding protein C partially rescues a cardiomyopathy phenotype in murine engineered heart tissue, Sci. Rep. 9 (2019) 18152.
[49] S. Huke, B.C. Knollmann, Increased myofilament Ca2+−sensitivity and arrhythmia susceptibility, J. Mol. Cell. Cardiol. 48 (2010) 824–833.
[50] E.R. Witjas-Paalberends, A. Guclu, T. Germans, P. Knaapen, H.J. Harms, A. M. Vermeer, I. Christiaans, A.A. Wilde, C. Dos Remedios, A.A. Lammertsma, A. C. van Rossum, G.J. Stienen, M. van Slegtenhorst, A.F. Schinkel, M. Michels, C. Y. Ho, C. Poggesi, J. van der Velden, Gene-specific increase in the energetic cost of contraction in hypertrophic cardiomyopathy caused by thick filament mutations, Cardiovasc. Res. 103 (2014) 248–257.
[51] J.G. Crilley, E.A. Boehm, E. Blair, B. Rajagopalan, A.M. Blamire, P. Styles, W. J. McKenna, I. Ostman-Smith, K. Clarke, H. Watkins, Hypertrophic cardiomyopathy due to sarcomeric gene mutations is characterized by impaired energy metabolism irrespective of the degree of hypertrophy, J. Am. Coll. Cardiol. 41 (2003) 1776–1782.
[52] S. Huke, R. Venkataraman, M. Faggioni, S. Bennuri, H.S. Hwang, F. Baudenbacher, B.C. Knollmann, Focal energy deprivation underlies arrhythmia susceptibility in mice with calcium-sensitized myofilaments, Circ. Res. 112 (2013) 1334–1344.
[53] E. Farrell, A.E. Armstrong, A.C. Grimes, F.J. Naya, W.J. de Lange, J.C. Ralphe, Transcriptome analysis of cardiac hypertrophic growth in MYBPC3-null mice suggests early responders in hypertrophic remodeling, Front. Physiol. 9 (2018) 1442.
[54] M.D. Lemoine, I. Mannhardt, K. Breckwoldt, M. Prondzynski, F. Flenner, B. Ulmer, M.N. Hirt, C. Neuber, A. Horvath, B. Kloth, H. Reichenspurner, S. Willems, A. Hansen, T. Eschenhagen, T. Christ, Human iPSC-derived cardiomyocytes cultured in 3D engineered heart tissue show physiological upstroke velocity and sodium current density, Sci. Rep. 7 (2017) 5464.
[55] A. Horvath, M.D. Lemoine, A. Loser, I. Mannhardt, F. Flenner, A.U. Uzun, C. Neuber, K. Breckwoldt, A. Hansen, E. Girdauskas, H. Reichenspurner, S. Willems, N. Jost, E. Wettwer, T. Eschenhagen, T. Christ, Low resting membrane potential and low inward rectifier potassium currents are not inherent features of hiPSC-derived Cardiomyocytes, Stem Cell Rep. 10 (2018) 822–833.
[56] M. Lemme, B.M. Ulmer, M.D. Lemoine, A.T.L. Zech, F. Flenner, U. Ravens, H. Reichenspurner, M. Rol-Garcia, G. Smith, A. Hansen, T. Christ, T. Eschenhagen, Atrial-like engineered heart tissue: an in vitro model of the human atrium, Stem Cell Rep. 11 (2018) 1378–1390.
[57] B.M. Palmer, D. Georgakopoulos, P.M. Janssen, Y. Wang, N.R. Alpert, D.F. Belardi, S.P. Harris, R.L. Moss, P.G. Burgon, C.E. Seidman, J.G. Seidman, D.W. Maughan, D. A. Kass, Role of cardiac myosin binding protein C in sustaining left ventricular systolic stiffening, Circ. Res. 94 (2004) 1249–1255.
[58] E. Brunello, L. Fusi, A. Ghisleni, S.J. Park-Holohan, J.G. Ovejero, T. Narayanan, M. Irving, Myosin filament-based regulation of the dynamics of contraction in heart muscle, Proc. Natl. Acad. Sci. U. S. A. 117 (2020) 8177–8186.
[59] S.P. Harris, Making waves: a proposed new role for myosin-binding protein C in regulating oscillatory contractions in vertebrate striated muscle, J. Gen. Physiol. 153 (2021).
[60] G. Captur, C.Y. Ho, S. Schlossarek, J. Kerwin, M. Mirabel, R. Wilson, S. Rosmini, C. Obianyo, P. Reant, P. Bassett, A.C. Cook, S. Lindsay, W.J. McKenna, K. Mills, P. M. Elliott, T.J. Mohun, L. Carrier, J.C. Moon, The embryological basis of subclinical hypertrophic cardiomyopathy, Sci. Rep. 6 (2016) 27714.

[61] P. Garcia-Canadilla, A.C. Cook, T.J. Mohun, O. Oji, S. Schlossarek, L. Carrier, W. J. McKenna, J.C. Moon, G. Captur, Myoarchitectural disarray of hypertrophic cardiomyopathy begins pre-birth, J. Anat. 235 (2019) 962–976.

[62] C.L. Huang, Murine electrophysiological models of cardiac arrhythmogenesis, Physiol. Rev. 97 (2017) 283–409.

[63] J.M. Nerbonne, Mouse models of arrhythmogenic cardiovascular disease: challenges and opportunities, Curr. Opin. Pharmacol. 15 (2014) 107–114.